Bioinspired Thermoresponsive Xyloglucan–Cellulose Nanocrystal Hydrogels

Malika Talantikite, Taylor Stimpson, Antoine Gourlay, Sophie Le-Gall, Céline Moreau, Emily Cranston, Jose Moran-Mirabal, Bernard Cathala

pubs.acs.org/Biomac

Article

Bioinspired Thermoresponsive Xyloglucan–Cellulose Nanocrystal Hydrogels

Malika Talantikite, Taylor C. Stimpson, Antoine Gourlay, Sophie Le-Gall, Céline Moreau, Emily D. Cranston, Jose M. Moran-Mirabal, and Bernard Cathala*

Cite This: *Biomacromolecules* 2021, 22, 743–753

Read Online

ACCESS | Metrics & More | Article Recommendations | Supporting Information

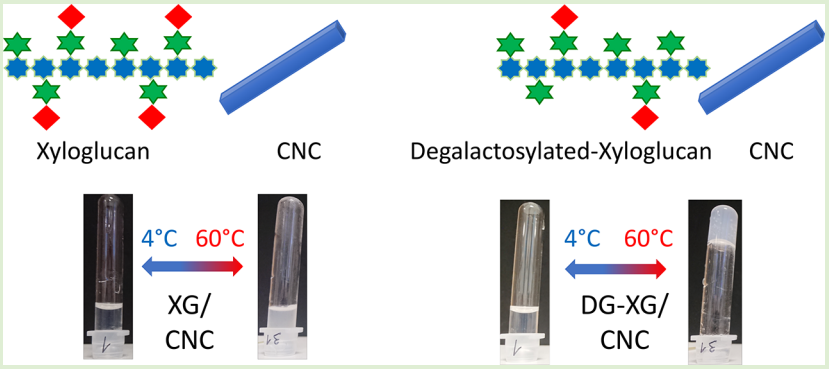

ABSTRACT: Thermoresponsive hydrogels present unique properties, such as tunable mechanical performance or changes in volume, which make them attractive for applications including wound healing dressings, drug delivery vehicles, and implants, among others. This work reports the implementation of bioinspired thermoresponsive hydrogels composed of xyloglucan (XG) and cellulose nanocrystals (CNCs). Starting from tamarind seed XG (XGt), thermoresponsive XG was obtained by enzymatic degalactosylation (DG-XG), which reduced the galactose residue content by ∼50% and imparted a reversible thermal transition. XG with native composition and comparable molar mass to DG-XG was produced by an ultrasonication treatment (XGu) for a direct comparison of behavior. The hydrogels were prepared by simple mixing of DG-XG or XGu with CNCs in water. Phase diagrams were established to identify the ratios of DG-XG or XGu to CNCs that yielded a viscous liquid, a phase-separated mixture, a simple gel, or a thermoresponsive gel. Gelation occurred at a DG-XG or XGu to CNC ratio higher than that needed for the full surface coverage of CNCs and required relatively high overall concentrations of both components (tested concentrations up to 20 g/L XG and 30 g/L CNCs). This is likely a result of the increase in effective hydrodynamic volume of CNCs due to the formation of XG-CNC complexes. Investigation of the adsorption behavior indicated that DG-XG formed a more rigid layer on CNCs compared to XGu. Rheological properties of the hydrogels were characterized, and a reversible thermal transition was found for DG-XG/CNC gels at 35 °C. This thermoresponsive behavior provides opportunities to apply this system widely, especially in the biomedical field, where the mechanical properties could be further tuned by adjusting the CNC content.

INTRODUCTION

Over the past few decades, there has been a focus on the fabrication of biobased structures with a low environmental footprint that simultaneously boast high mechanical performance associated with responsive or switchable behaviors. With this aim, biological structures, such as those in the primary plant cell wall, can be a source of inspiration. In nature, the plant cell wall provides strategies and exquisitely designed assemblies, which allow the association of a soft matrix and hard materials that result in impressive and tunable properties.

The primary plant cell wall is composed of cellulose, hemicelluloses, and pectin, which form an intricate swollen network that can be described as a hydrogel. In the primary cell wall, the cellulose component exists as a collection of long microfibrils, with nanoscale transverse dimensions, that are in close association with hemicelluloses, such as xyloglucan (XG). The exact role of XG *in planta* is still a matter of debate, but it has been proposed that it acts both as a tether between cellulose microfibrils as well as a polymer coil that influences the mechanical behavior of the plant cell wall.[1,2] Nevertheless, interactions between cellulose and XG have been widely

Received: October 22, 2020
Revised: December 6, 2020
Published: December 17, 2020

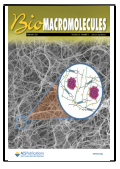

studied for decades,[2−4] and XG adsorption to cellulose surfaces is now understood as an entropically driven process that can be modulated by kinetic effects and/or by the limited solubility of hemicelluloses in water.[5−8]

The nanoscale characteristics of the cellulose microfibrils in the plant cell wall can be mimicked by isolating nanocelluloses for *in vitro* studies or for the implementation of bioinspired materials.[9−13] Nanocelluloses are a class of sustainable nanomaterials that can be divided into two categories: cellulose nanofibrils (CNFs) and cellulose nanocrystals (CNCs). The latter corresponds to the crystalline regions of the cellulose microfibrils that can be isolated through acid hydrolysis or oxidation. CNCs are high aspect ratio rod-shaped nanoparticles that have been used in many applications due to their excellent mechanical properties, colloidal and thermal stability, ability to stabilize emulsions and foams, and low toxicity.[14−16] These properties make CNCs excellent candidates to be used as building blocks for various hydrogel materials.[17]

Hydrogels are three-dimensional water-swollen networks formed through chemical bonding or physical interactions between polymers and/or particles. They are used in industrial applications such as personal care products, food, and pharmaceuticals as well as in the field of regenerative medicine.[18] Hydrogels, in most of the cases, are composed of a single polymer that can be covalently or not cross-linked. A way to enhance hydrogel properties is the implementation of more complex mixtures, and an elegant strategy is to take advantage of self-assembly capabilities of polymer/nanoparticle systems. Indeed, hydrogels composed of nanoparticles and polymers display enhanced properties such as efficient tunable and self-healing properties, high water content, and moldability or strong and rapid adhesion.[19−22] However, the mechanism of the formation of polymer/nanoparticle hydrogels, and more specifically those made from a mixture of CNCs and polymers, remains still to be investigated in depth; these systems are complex because gelation can arise either from depletion forces or from polymer−CNC interactions that result in cross-linking or gel stabilization through steric hindrance.[17,23−25]

Among other amazing functional properties, hydrogels can present thermoresponsive behaviors when they are composed of polymers displaying abrupt changes in solubility in response to an increase in temperature. This behavior is also termed a lower critical solution temperature (LCST) and is generally viewed as a phenomenon governed by the balance of hydrophilic and hydrophobic moieties within a polymer. Some natural polymers display such responsive behavior, among which polysaccharides are a class of interest due to their large availability and structural versatility.[26−29] In addition to its affinity for cellulose, XG can also display thermoresponsive behavior when appropriate structural modification is achieved. The XG backbone is typically arranged in blocks of four successive glucose units, three of which carry a flexible α-(1,6)-linked D-xylosyl substituent that can be modified to yield β-D-Gal-(1,2)-α-D-Xyl side chains. Partial removal of galactose residues results in degalactosylated XG (DG-XG), which has been reported to exhibit thermoresponsive behavior.[30] Conversely, CNC-based thermoresponsive hydrogels have also been previously reported and are generally obtained through CNC surface functionalization via either chemical grafting or adsorption with thermoresponsive polymers.[31−35] However, to the best of our knowledge, there are no reports of thermoresponsive hydrogels obtained by a straightforward green method, such as combining XG and CNCs through simple mixing. Inspired by the strong specific interactions between XG and CNCs, our aim was to investigate the thermoresponsive behavior of Tamarind seed polysaccharide/nanocellulose hydrogels consisting of hard, reinforcing colloidal CNCs and soft XGu or DG-XG polymers.

EXPERIMENTAL SECTION

Materials. CNCs purchased from CelluForce (Canada) were obtained as a spray-dried powder in the sodium salt form. CNCs were produced by sulfuric acid hydrolysis of bleached kraft pulp. According to product specifications, the CNCs have a particle cross section of 2.3−4.5 nm (by atomic force microscopy, AFM), particle length of 44−108 nm (by AFM), crystalline fraction of 0.88 (by X-ray diffraction), and sulfate content of 246−261 mmol/kg, in agreement with previous reports.[36] Tamarind seed polysaccharide (XGt) was purchased from DSP Goyko Food & Chemical (Japan) and was precipitated in ethanol before use to remove low molecular weight impurities, especially glucose. β-Galactosidase from *Aspergillus oryzae* was purchased from Sigma-Aldrich (USA).

Preparation of Degalactosylated Xyloglucan (DG-XG). Enzymatic modification of XGt was performed according to the protocol of Brun-Graeppi et al.[37] Modification of 2 g of 20 g/L XGt was performed at pH 5 (phosphate buffer) and 50 °C with an enzyme:substrate ratio of 0.37 U/mg XGt. The starting transparent solution was left to stir for 22 h, becoming progressively cloudy as the reaction proceeded. The reaction was cooled by stirring in an ice bath. As the temperature decreased, the solution became transparent again. The resulting DG-XG solution was poured into 400 mL of cold ethanol. The precipitate was vigorously stirred, filtered, washed with ethanol and diethyl ether, then dried in a crystallization dish under ambient conditions.

Preparation of Ultrasonicated Xyloglucan (XGu). XGt was subjected to ultrasonication to obtain polymers with reduced molar mass (XGu).[7] XGt solution (200 mL at 10 g/L) was sonicated for 40 min at 25% of the maximum amplitude by using a Q700 sonicator (20 kHz, 700 W maximum output, Qsonica LLC, Newtown, CT) with a 12.5 mm diameter titanium microtip. Every 5 min, the solution was homogenized by magnetic stirring. The final XGu solution was dialyzed (dialysis tube molecular weight cutoff of 3.5 kDa) and freeze-dried.

Preparation of CNC Suspensions and XGt, XGu, and DG-XG Solutions. A CNC suspension was prepared by dispersing powdered CNCs in deionized water (18.2 MΩ cm resistivity, Millipore Milli-Q purification system). The 30 g/L suspension (150 mL) was sonicated for 5 min at 50% amplitude, with an ultrasonic probe (Q700 sonicator, 20 kHz, QSonica LLC., Newtown, USA) equipped with a 12.5 mm diameter titanium microtip. XG solutions were prepared by dissolving the different XG fractions (XGt, DG-XG, and XGu) into deionized water. The XGt and XGu solutions were prepared by stirring at 40 °C, while the DG-XG solution was mixed at 4 °C (to prevent gelation).

Carbohydrate Analysis. Identification and quantification of neutral sugars of the different XG samples (XGt, DG-XG, and XGu) were performed by gas chromatography after sulfuric acid degradation. Each XG sample (5 mg) was dispersed in 13 M sulfuric acid for 30 min at 30 °C and then hydrolyzed in 1 M sulfuric acid (2 h, 100 °C). Sugars were converted to alditol acetates according to Blakeney et al.[38] and chromatographed in a TG-225 GC column (30 m × 0.32 mm ID) using a TRACE Ultra gas chromatograph (Thermo Scientific; temperature 205 °C, carrier gas H_2). A standard sugar solution and inositol as internal standard were used for quantification. After degalactosylation treatment, the galactose residue release (GRR) was determined according the following calculation: GRR = (% Gal_{XGt} − %$Gal_{DG\text{-}XG}$)/%Gal_{XGt} × 100.

High-Performance Size-Exclusion Chromatography (HPSEC). XG samples were dissolved at 5 g/L in 50 mM $NaNO_3$ (99% Sigma Ultra S8170-250G) and filtered at 0.1 μm before measurement. The eluent consisted of 50 mM $NaNO_3$ containing 0.02% NaN_3 and was filtrated through a 0.1 μm pore membrane. The

https://dx.doi.org/10.1021/acs.biomac.0c01521
Biomacromolecules 2021, 22, 743−753

samples were eluted at 0.6 mL/min on a Shodex OHpak SB-805 HQ column (8 mm × 300 mm). The online molar mass, refractive index, and intrinsic viscosity were measured by a multiangle laser light scattering (MALLS) detector (mini-Dawn, Wyatt, USA), a differential refractometer (ERC 7517 A), and a differential viscometer (T-50A, Viscotek, USA), respectively.[39] Molar masses were determined by using ASTRA 1.4 software (Wyatt, USA). The concentrations of eluted xyloglucans were calculated by using a refractive index increment dn/dc = 0.147 mL/g. This method allows a more accurate determination of peak concentrations and thus of molar mass.

Quartz-Crystal Microbalance with Dissipation (QCM-D). QCM-D measurements were performed by using a Q-Sense E4 instrument (Sweden) with piezoelectric AT-cut quartz crystal sensors coated with gold electrodes (QSX301, Q-Sense). A driving voltage was applied across the gold electrodes at the fundamental frequency of f_0 = 5 MHz. Frequency and dissipation changes were measured for the third, fifth, and seventh (n = 3, 5, and 7) harmonics simultaneously. Frequency and dissipation changes were normalized to the harmonic number (n). Because materials that adsorb to the sensor surface induce a decrease in the resonance frequency (f), the amount of material adsorbed can be related to the change in frequency ($\Delta f/n$).

To study the adsorption of different XG types to CNCs, XGu and DG-XG were adsorbed onto CNC-coated sensors and measured by QCM-D. Gold-coated quartz crystals were first cleaned with piranha solution (3:1 H_2SO_4:H_2O_2) for 15 min and rinsed with ultrapure water. The cleaned sensors were spin-coated (Spin 150 wafer spinner, accelerated at 180 rpm/s to 3600 rpm for 60 s) with an anchoring layer of poly(allylamine hydrochloride) (PAH, 4 g/L). A 30 g/L CNC suspension was then dropped onto PAH-coated sensors and allowed to adsorb for 5 min before spin coating at 3600 rpm for 60 s. Freshly prepared CNC-coated quartz crystal sensors were then placed in the QCM-D modules and equilibrated at 4 °C, while flowing deionized water over the sensors for 1 h to establish a stable baseline (<1−2 Hz shift over 15 min) in the frequency response. Either XGu or DG-XG at different concentrations (0.01, 0.1, and 1 g/L) were injected at 50 μL/min and allowed to adsorb onto the CNC-coated sensors for 1 or 16 h. After the adsorption step, water was injected for 10 min to remove any loosely bound XGu or DG-XG. Normalized frequency shifts for the third harmonic were directly compared.

Inverted Test Tube Method for Phase Diagram. To obtain phase diagrams, mixtures of different ratios of XGu or DG-XG and CNCs were prepared at ambient temperature by varying the concentrations of XGu or XG-DG (0−20 g/L) and CNCs (0−30 g/L) to produce final volumes of 3 mL. The mixtures were vortexed before putting them in a cold room at 4 °C or in a water bath at 60 °C for a few minutes, and then the inverted test tube method was performed for each sample by turning the tube upside down to submit it to its own weight. Gelation was visually determined by assessing whether the mixtures flowed or not, 5 min after mixing. The reversibility of the sol−gel transition was evaluated by submitting samples to alternating high (60 °C) and low (4 °C) temperature, ten times successively.

Rheology. Rheological measurements were performed by using a stress-controlled rheometer AR-2000 (TA Instruments) equipped with a truncated cone (40 mm diameter, 2° cone). The storage (G') and loss (G'') moduli were measured at an angular frequency of 1 Hz. The imposed stress was chosen within the linear response regime. Temperature ramps were performed by using a rate of 0.5 °C/min. Samples were covered with paraffin oil to prevent sample evaporation. Samples were submitted to two heating/cooling cycles and displayed reproducible behavior.

Polarized Optical Microscopy (POM). POM was performed by using an upright Olympus system microscope (Model BX51) with crossed polarizers and a 530 nm retardation plate (U-TP530). Digital images were taken of samples between the microscopy slide and the cover glass by using a Sony XCD-SX90CR charge-coupled device camera. The microscope was equipped with a HS82 heated stage (METTLER TOLEDO) allowing temperature control under the microscope.

RESULTS AND DISCUSSION

Enzymatic Modification of Xyloglucan and Characterization. Previous studies have reported that a partial removal (typically 20−40%) of the galactose substituent of XG leads to thermally induced gelling properties.[30,37,40,41] According to the protocol of Brun-Graeppi et al., a 2% solution of XGt was mixed with β-galactosidase at 50 °C.[37] Selective removal of the galactose moieties induced thermoresponsive behavior (Figures 1a,b). As the reaction proceeded, the solution

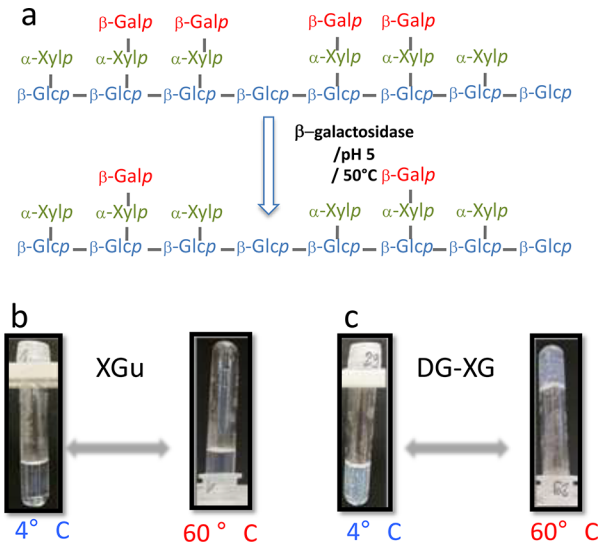

Figure 1. Enzymatic modification of XGt by β-galactosidase (a). Inverted test tube assay for XGu (b) and DG-XG (c) at 4 and 60 °C. XGu remains a liquid at both temperatures while DG-XG becomes a gel at high temperatures. All measurements were performed with 20 g/L XGu or DG-XG.

progressively turned into a gel-like phase since the reaction temperature was higher than the LCST. Cooling the mixture at the end of the reaction reversed the gelation, turning the mixture back to a liquid in a transparent state. This experiment suggests that degalactosylated XGt displays thermoresponsive behavior. Nevertheless, before evaluating the functionality of the modified DG-XG, we investigated the structure and composition of native and modified XG types.

The monosaccharide composition of XGt was determined and is reported in Table 1. Native XGt is composed of glucose, xylose, and galactose. After the enzymatic reaction with β-galactosidase, the galactose content was significantly decreased (∼16% dry weight for XGt vs ∼8% dry weight for DG-XG), confirming β-galactosidase activity during enzymatic modification. In addition to monosaccharide composition, we also monitored the molar mass of XG before and after degalactosylation, since molar mass is a key parameter for rheological properties, interactions between XG and cellulose, and gelation behavior. HPSEC was used to investigate the macromolecular characteristics of the native and modified XG types. The starting weight-average molar mass (M_w) of XGt was in the range of 8.4 × 10^5 g/mol, which agrees with earlier results from our group and others.[7,37,41] After degalactosylation, M_w was found to be significantly lower, in the range of 3.3 × 10^5 g/mol. A similar trend was previously reported for XGt that had undergone a degalactosylation reaction,[37,41] and the lower molar mass was mainly attributed to aggregation that could reduce the solubility of the largest XGt chains, resulting

https://dx.doi.org/10.1021/acs.biomac.0c01521
Biomacromolecules 2021, 22, 743−753

Table 1. Monosaccharide Composition (Dry Weight %), Galactose Residue Release (GRR), Weight- and Number-Average Molar Mass (M_w and M_n), Radius of Gyration (R_g, nm), and LCST (°C) of Native XGt, XGu, and DG-XG[a]

	Xyl (wt %)	Gal (wt %)	Glc (wt %)	GRR (%)	M_w (10^3 g/mol)	M_n (10^3 g/mol)	R_g (nm)	LCST (°C)
XGt	32.7 ± 0.9	16.1 ± 0.3	51.0 ± 0.4	0	840	674	72	
XGu	31.2 ± 0.8	15.6 ± 0.2	51.4 ± 0.3	0	326	214	32	
DG-XG	34.1 ± 0.7	8.2 ± 0.1	57.6 ± 0.3	49	303	224	42	35

[a]Figure S1 displays HPSEC traces and molar mass distribution.

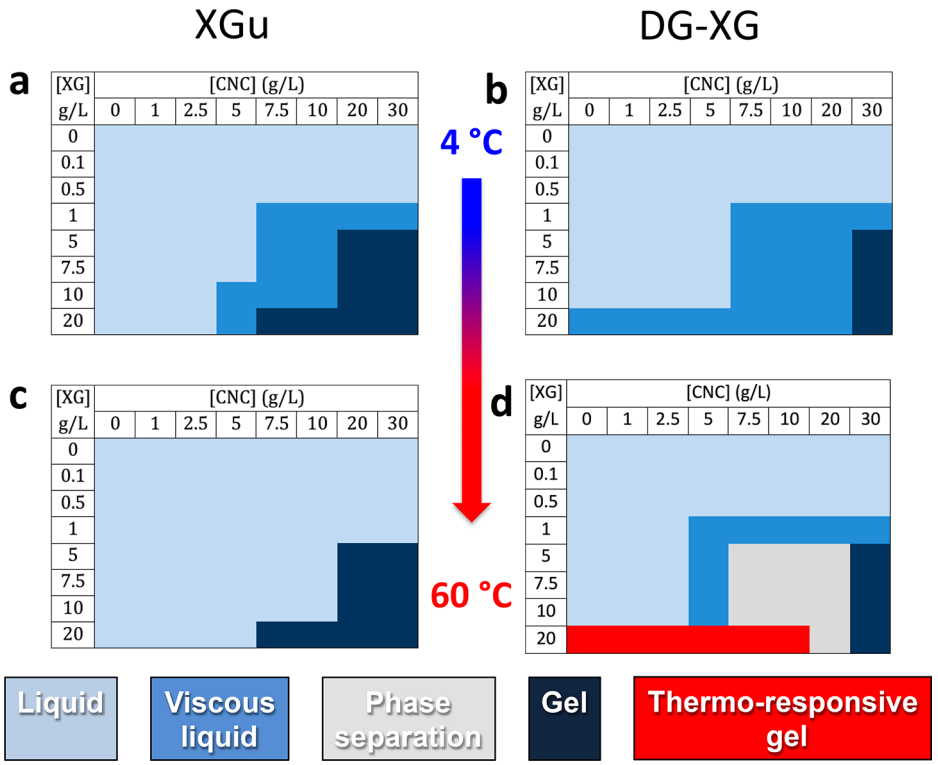

Figure 2. Phase diagrams determined by the inverted test tube method for XGu (a, c) and DG-XG (b, d) mixed with CNCs at different ratios and at 4 °C (a, b) and 60 °C (c, d). Representative images of the different phases observed are displayed in Figure S3.

in a selection of molecules that tended toward lower molar mass. However, in our case, the recovery yield in HPSEC remained high (recovery was ~80% for XGt and XGu and ~70% for DG-XG), suggesting that the degalactosylated sample as a whole presented a lower mass than the starting material. In light of these results, we cannot rule out the presence of contaminant endoglucanase activity in the enzyme mixture used, which could induce chain cleavage or elimination of high molar mass fractions during the degalactosylation reaction and purification.

Because molar mass is a critical parameter known to affect XG-CNC interactions and gelation,[7,42] we prepared a XG with a similar molar mass to that of the DG-XG. To accomplish this, XGu was prepared by ultrasonication according to a previously reported procedure.[7,42] By careful adjustment of the dwell time and the ultrasonic energy input, it was possible to achieve accurate fractionation and prepare a sample with M_w and M_n values that closely match DG-XG (Table 1). Nevertheless, it should be noted that R_g of DG-XG was slightly higher than that of XGu. This variation can be attributed to a change in the XG polymer chain conformation due to removal of galactose moieties. Thus, for relevant comparison between polymers with similar molar mass XGu, rather than XGt, and DG-XG were selected for the results presented in the next sections.

We investigated the rheological behavior of XGu, which has a high galactose content, and DG-XG, which has approximately half the amount of galactose (GRR = 49%, Table 1). Brun-Graeppi et al. have studied the relationship between the GRR and the thermal gelation of degalactosylated XG in prior work.[37] Reversible gelation was observed when the GRR reached a value of about 30%, where a decreasing LCST was observed with increasing GRR. Our investigation of the rheological temperature dependence of the XG samples at 20 g/L indicated a crossover of the storage (G') and loss (G'') moduli at 35−40 °C (corresponding to the LCST and point of gelation) in the case of DG-XG (Supporting Information, Figure S2). In contrast, G'' remained higher than G' at all temperatures for XGu (Figure S2). Cooling the DG-XG sample decreased the G' value with hysteresis from the heating curve likely due to a cooperative process of chain association that would speed up the gelation process and slow down the dissociation process. Nevertheless, the gel−sol transition occurred, confirming the reversibility of gelation (Figure S2). The sol−gel transition was also qualitatively demonstrated by the inverted test tube method. After heating to 60 °C, the DG-XG solution did not flow (Figure 1c) while the solution of XGu remained a liquid (Figure 1b).

Evaluation of CNC/XGu and CNC/DG-XG Interactions. Figure 2 presents the phase diagrams for XGu/CNC (Figures

https://dx.doi.org/10.1021/acs.biomac.0c01521
Biomacromolecules 2021, 22, 743−753

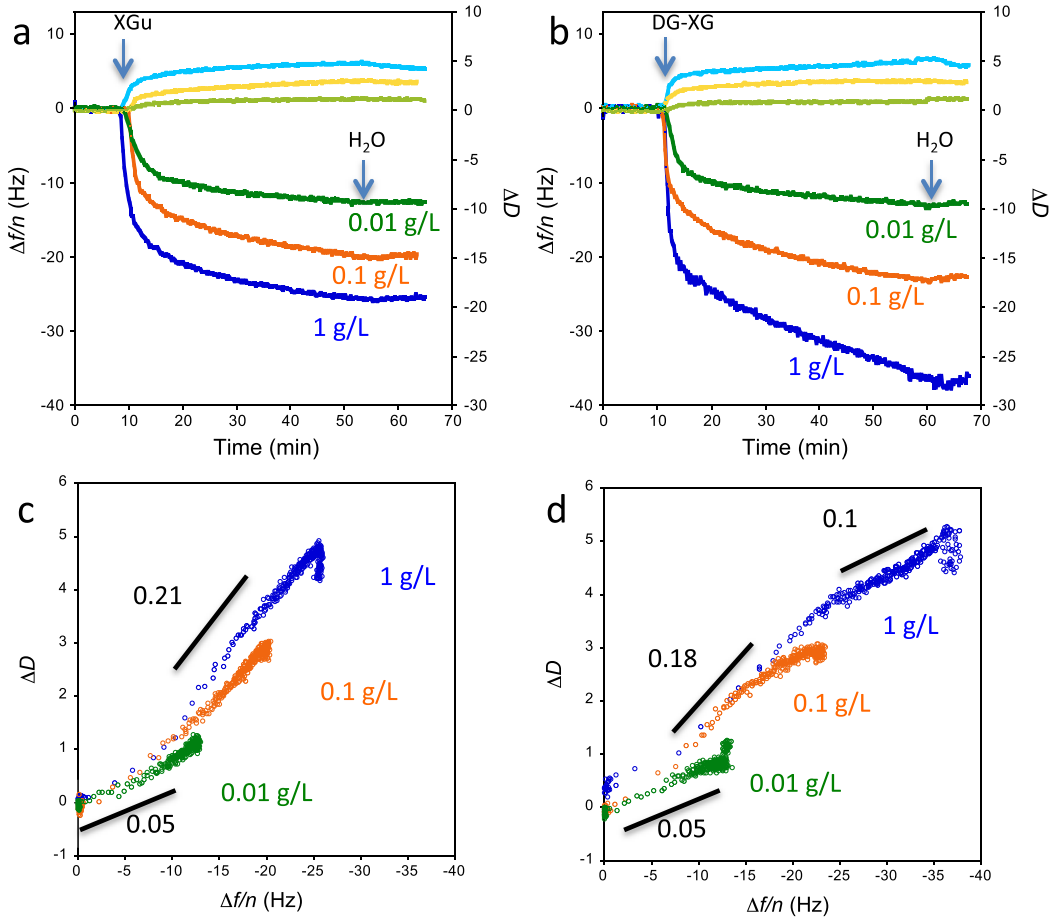

Figure 3. QCM-D traces of XGu and DG-XG adsorption onto CNC-coated sensors. Normalized frequency ($\Delta f/n$) and dissipation (ΔD) traces vs time for the third harmonic for XGu (a) and DG-XG (b) aqueous solutions injected at different concentrations: 0.01 g/L light green (dissipation) and dark green (frequency); 0.1 g/L yellow (dissipation) and orange (frequency); and 1 g/L light blue (dissipation) and dark blue (frequency). The arrows indicate when XGu and DG-XG samples were injected and the rinsing step with deionized water. Dissipation as a function of normalized frequency change for XGu (c) and DG-XG (d) is shown at three concentrations: 0.01 g/L (green), 0.1 g/L (orange), and 1 g/L (blue). Black lines are to guide the eye and indicate the different slopes observed.

2a,c) and DG-XG/CNC (Figures 2b,d) mixtures at different concentration ratios and at two temperatures (4 °C, Figures 2a,b; 60 °C, Figures 2c,d). The phase diagrams were obtained from qualitative observations of the inverted test tube assays. Several phases were identified and classified as (1) liquid, when the mixture flows easily; (2) viscous liquid, when the mixture flowed slowly along the wall of the tube; and (3) gel, when the mixture did not flow under its own weight during inversion (Figure S3). In the case of DG-XG/CNC, an additional fourth phase consisting of phase separation was identified, where upon heating the mixture went from translucent to milky and two distinct phases could be seen during inversion. We note that CNC suspensions on their own did not gel in the concentration range examined (0−30 g/L) as their gelation concentration is known to be significantly higher.[43] This indicates that the gels formed as a result of physical interactions between CNCs and XGu or DG-XG.

The phase diagrams for the XGu/CNC mixtures are very similar at 4 and 60 °C. The main difference between the phases across the two temperatures is the transition from a viscous liquid to liquid, indicating a decrease in viscosity with increased temperature. Gelation occurs at high CNC and XG concentrations for both XGu and DG-XG, suggesting that the XG-CNC interactions induce the formation of a network (30 g/L CNCs, Figure 2). Hydrogel stabilization is reminiscent of our recent results obtained on arabinoxylan/CNC mixtures; in this system, stabilization resulted from a combination of the steric repulsion between arabinoxylan/CNC complexes due to arabinoxylan chain/chain interactions, the electrostatic repulsions due to the surface charges of CNCs, and associative interactions between arabinoxylans/CNC complexes mediated by arabinoxylan chains.[42] This mechanism mirrors that of attractive glasses, in which both attractive and repulsive interactions are significant but where the repulsive interactions dominate.[44] Furthermore, dilution does not induce the breaking of the gel, suggesting that hemicellulose/nanocellulose gel systems are different from the volume-arrested state observed in the gelation of pure nanocellulose.[45] Phase diagrams for DG-XG/CNC mixtures are more complex and differ from those of XGu/CNC. At 4 °C, gelation occurs only at the highest CNC concentration tested, suggesting that degalactolysation effectively changed the architecture of the network. This part of the phase diagram remains unchanged when the temperature is increased. However, two notable changes can be seen for the other DG-XG/CNC ratios. First, a phase separation domain appeared at intermediate concentrations of CNCs and DG-XG (gray zone, Figure 2d). Increasing the temperature introduced the appearance of

https://dx.doi.org/10.1021/acs.biomac.0c01521
Biomacromolecules 2021, 22, 743−753

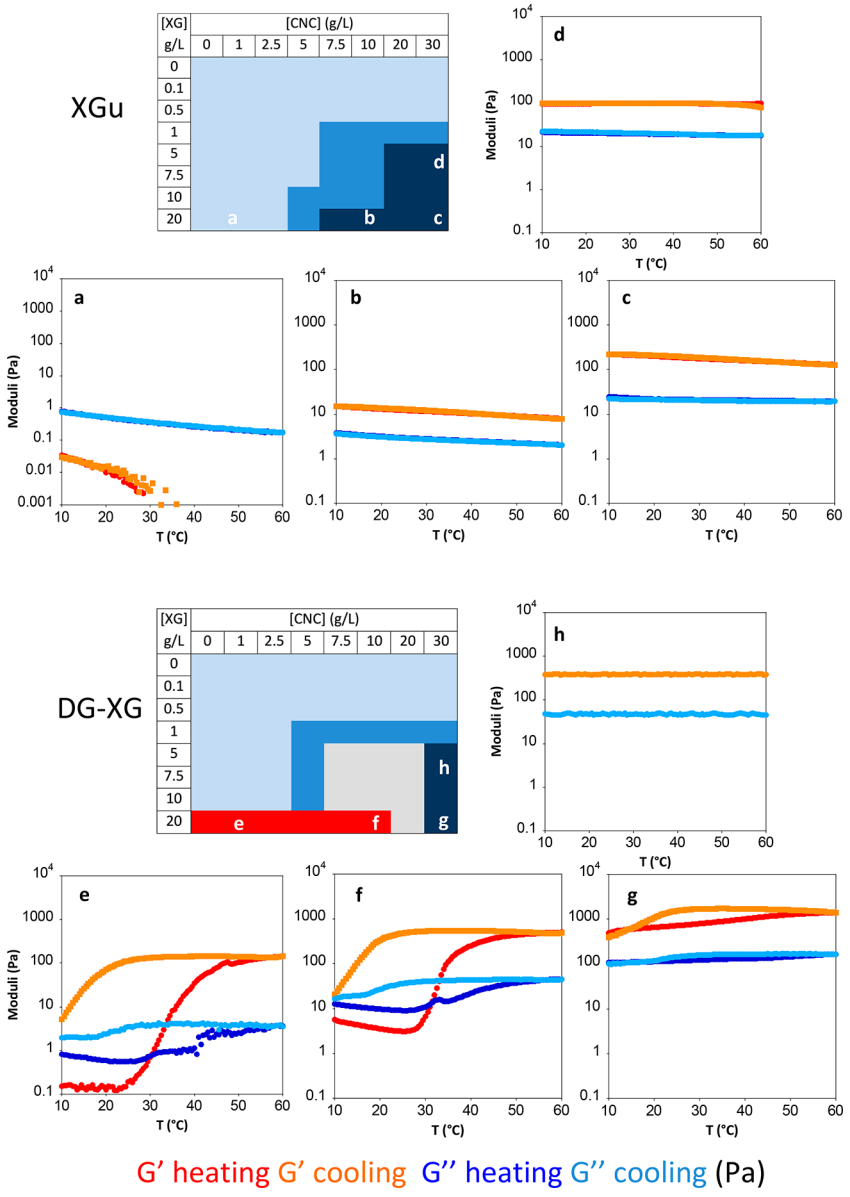

Figure 4. Temperature dependence of the storage (G') and loss (G'') moduli for different CNC and XGu/DG-XG concentrations. The phase diagrams at 60 °C in Figure 2 are shown again with the various regions labeled a−h which correspond to the respective rheology plots. Typical G' and G'' values are reported in Table S1.

particles that settled out of suspension. Remarkably, the phase separation did not disappear when the mixtures were cooled, suggesting the formation of large irreversible aggregates. Second, a thermoresponsive gel phase was formed at 20 g/L DG-XG with CNC concentrations below 20 g/L (red zone, Figure 2d). The gel was formed only at high temperature, which transitioned back to a viscous liquid when the mixture was cooled. Temperature cycling resulted in the transition between liquid and gel, demonstrating that reversible thermoresponsive DG-XG/CNC hydrogels can be achieved.

These results raise the question of how the interactions between CNCs and DG-XG compare to those between CNCs and XG variations with a higher degree of galactosylation. The XGu/CNC and DG-XG/CNC interactions were investigated by monitoring XGu and DG-XG adsorption profiles on CNC surfaces through QCM-D experiments. The two XG variants (XGu and DG-XG) were adsorbed onto CNC-coated QCM-D sensors, as previously described.[6,7] Adsorption experiments were run at low temperature (4 °C) to avoid any gelation and subsequent clogging of the QCM-D microfluidic channels. For both XGu and DG-XG, at all injection concentrations, it was observed that immediately after injection the frequency dropped and the dissipation increased (Figures 3a,b), indicating fast polymer adsorption to the CNC films. However, the adsorption trends observed for XGu and DG-XG display clear differences.

In the case of XGu, the frequency signal stabilized in <1 h while the DG-XG signal only stabilized after 1 h for the lowest concentration tested (0.01 g/L). For the two higher concentrations (0.1 and 1 g/L), stabilization occurred after several hours of continuous injection despite 80−90% of the adsorption occurring in the two first hours (Figure S4). Water injection (i.e., rinsing) did not induce a substantial change in the frequency value for any of the samples, indicating that the adsorption onto the CNC surface was irreversible for both XGu and DG-XG. Similar final frequency shift values (−12

https://dx.doi.org/10.1021/acs.biomac.0c01521
Biomacromolecules 2021, 22, 743−753

Hz) were obtained for the lowest XGu and DG-XG concentrations (0.01 g/L). Conversely, significantly different values were measured for the higher concentrations, where $\Delta f/n$ reached −20 and −25 Hz for XGu and −31 and −52 Hz for DG-XG for 0.1 and 1 g/L concentrations, respectively (Figure 3 and Figure S4). Differences in the final surface concentration according to the injected concentration have been reported previously for the adsorption of hemicelluloses to cellulose, whereby both kinetic and thermodynamic adsorption mechanisms explain the differences observed.[6−8] Overall, at higher XG concentrations, more DG-XG adsorbed to the CNC-coated surface than XGu.

To further contrast the adsorption behavior of DG-XG and XGu, we plotted the change in dissipation as a function of the normalized frequency shift to remove time as an explicit parameter (Figures 3c,d). At low frequency shifts, the slope $\Delta D/(\Delta f/n)$ is small, suggesting the adsorption of a relatively rigid layer with lower hydration. The slopes measured are identical for both XGu and DG-XG (0.05 Hz^{-1}). At higher frequency shifts (10 Hz < $\Delta f/n$ < 20 Hz), the increase in slope indicates the formation of a more viscous layer. This is likely linked to a more hydrated layer and a conformational change of the adsorbed polymer chains, from an extended and less hydrated conformation to a more hydrated layer with loops and tails. The slope is slightly lower for DG-XG than for XGu (0.18 vs 0.21 Hz^{-1}), suggesting the formation of a more rigid structure on CNCs in the case of the partially degalactosylated sample. In the earlier stages of absorption, the interaction between DG-XG and CNCs appears to exhibit a tighter association compared to XGu and CNCs, likely because the XG backbone can more easily interact with the cellulose surface when fewer galactose side chains are present. For frequency shifts up to −25 Hz, interactions between XG chains may play a more significant role, and DG-XG continues to form denser (more tightly packed) layers, as noted from the smaller slope compared to XGu. One explanation for this behavior is that the degalactosylated regions could promote chain association between DG-XG loops and tails, resulting in increased number of contact points forming a denser network. In contrast, the self-association of XGu is less favorable; the presence of galactose substituents that sterically hinder interactions between neighboring XGu chains results in fewer contact points and therefore a less dense network. This assumption is supported by rheology investigations that report only weak interactions between XGt or XGu chains with higher galactose content than DG-XG.[46]

Rheological Properties of Hydrogels. The rheological behavior of XGu/CNC and DG-XG/CNC mixtures was investigated for different regions of the phase diagram, with a focus on the evolution of the storage (G') and loss (G'') moduli as a function of temperature, to characterize the thermoresponsive properties of the mixtures (Figure 4). In all cases, the CNC concentrations used for these experiments were far below the expected limit of CNC gelation.[43] It has also been reported previously that temperature has little effect on the rheological properties of CNC suspensions.[43] However, upon mixing the different types of XG with CNCs, gelation and a temperature dependence were observed.

In the first region (Figures 4a−c for XGu and Figures 4e−g for DG-XG), the CNC concentration was increased while concentrations of both types of XG were kept constant at 20 g/L. This section of the phase diagram (Figure 2) is in agreement with previous work, which showed that unmodified XGt does not display thermal sensitivity at concentrations of up to 20 g/L.[37] The second region (Figures 4c,d for XGu and Figures 4g,h for DG-XG) corresponds to a constant CNC concentration of 30 g/L and two different XG concentrations (5 and 20 g/L). At these concentrations, the XG/CNC mixtures formed a gel at both low and high temperatures.

Mixtures of CNCs with XGu, which has a high degree of galactose side chains, resulted in gel formation at high XGu/CNC ratios and concentrations, in agreement with our recently reported results.[42] An increase of the mechanical properties of the gel was observed, as expected, during the temperature sweep. At low CNC concentration, specifically for 1 g/L CNCs and 20 g/L XGu (Figure 4a), the mixture behaved as a liquid; G'' displays a higher value than G'. Increasing the CNC concentration led to gel formation, which is demonstrated by the higher G' value compared to G'' (Figures 4b,c) and agrees with the inverted test tube results. Increasing the CNC concentration 3-fold (from 10 to 30 g/L) induced a 13-fold increase in G' (from 10 to 130 Pa), illustrating the reinforcing effect of CNCs. In the case of the second region of the phase diagram (Figures 4c,d), gelation occurred for all XGu concentrations >5 g/L, since G' is higher than G'' at all temperatures. From these results, it appears that gelation of XGu/CNC mixtures requires two conditions:

(1) A XGu/CNC ratio higher than the ratio needed for the full surface coverage of CNCs. Indeed, we previously reported the XG adsorption isotherm on CNC and the surface saturation concentration can be estimated to 200−250 mg XG/g CNCs.[47] In all the conditions where gelation occurs, XGu is in excess compared to CNCs' surface availability, suggesting that CNCs' surfaces are crowded.

(2) A simultaneous high concentration of both CNCs and XGu. Gelation does not occur if XGu and CNC concentrations are too low.

This suggests that gelation is likely linked to the formation of XGu-CNC complexes mediated by XGu adsorption onto the CNC surface, which increases the effective hydrodynamic volume as suggested in previous studies.[23,42] At this point the role nanoparticle/polymer self-assembly should be emphasized as an efficient strategy to achieve hydrogel materials without the need of a complex synthetic approach. The use of high aspect ratio nanoparticles such as CNCs should favor steric crowding, leading to gel formation associated with a high affinity of XG for the cellulose surface, which might be an important driving force of the gel formation. Indeed, polymer adsorbed layers on nanoparticles increase tremendously the effective volume fraction of the particle and the rigid core, leading to stiff supramolecular complexes displaying steric hindrance.[48−50]

Mixing DG-XG and CNCs reveals more complex behavior than that of XGu/CNC mixtures. When the concentration of DG-XG is kept constant at 20 g/L and the CNC concentration is varied, at low temperature only the highest CNC concentration (30 g/L) resulted in gel formation (Figure 4g). For the lower CNC concentrations tested (Figures 4e,f), G' crossed over G'' during the course of the temperature sweep, indicating a change in the mechanical behavior from liquid to solidlike. Even at the highest CNC concentrations, a small but noticeable jump in G' occurred (Figure 4g). Furthermore, increasing the CNC concentration did not influence the LCST value (35 °C) compared to DG-XG

https://dx.doi.org/10.1021/acs.biomac.0c01521
Biomacromolecules 2021, 22, 743−753

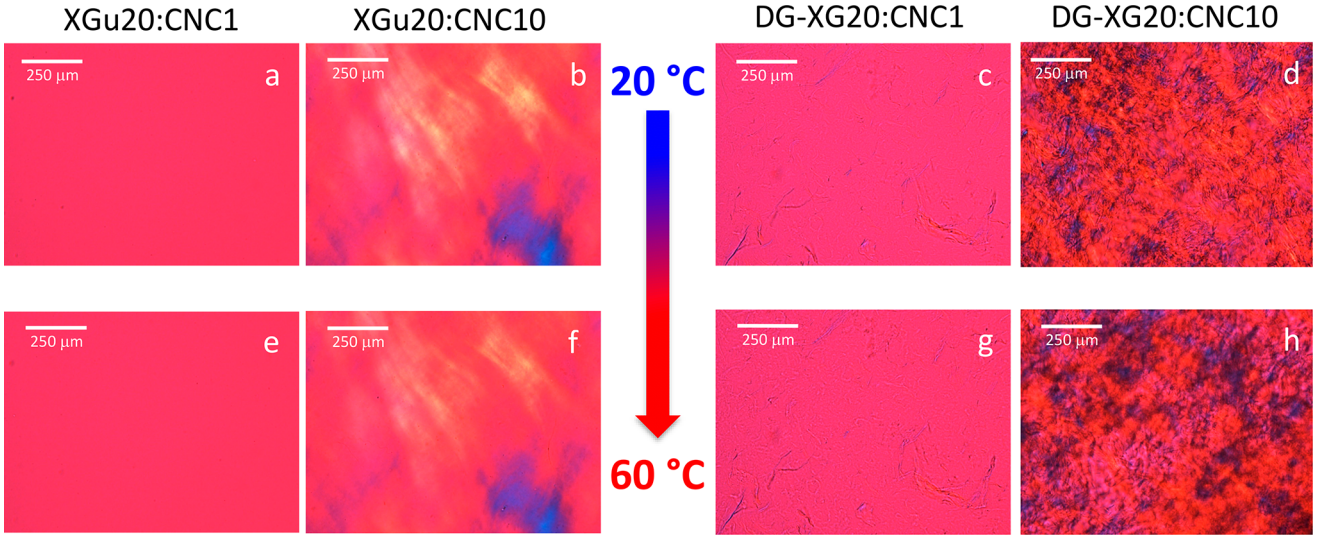

Figure 5. Polarized optical microscopy images of XGu/CNC (a, b, e, f) and DG-XG/CNC (c, d, g, h) mixtures at low (a, b, c, d) and high (e, f, g, h) temperature for ratios of 20:1 and 20:10 (XG/CNC).

alone (Figure 1). Temperature cycling also demonstrated the reversibility of the gelation process, where the kinetics appear to be close to those of DG-XG alone. This implies that the thermoresponsive properties of the hydrogels are strongly linked to DG-XG self-association, and interactions between CNCs and DG-XG do not modify the thermal transition value. The thermoresponsive properties of these materials are within a range of temperatures that could be of interest for biomedical applications (i.e., close to body temperature).

Increasing the CNC concentration also led to a higher G' at the plateau value after the thermal transition. G' is upward of 1000 Pa (Figure 4g) compared to values 10 times lower for the lowest concentration of CNCs (Figure 4e). It should also be noted that for similar mixture concentrations the G' values in all cases are significantly higher for DG-XG/CNC than for XGu/CNC, suggesting that DG-XG/DG-XG interactions are more efficient and more effectively strengthen the hydrogel network. This observation is in agreement with the greater adsorption and more rigid layer of DG-XG than XGu on CNCs as measured by QCM-D. Comparison of the highest CNC concentration at two DG-XG concentrations (Figures 4g,h) reveals different behaviors. The addition of 5 g/L DG-XG to 30 g/L of CNCs led to gel formation; however, no mechanical transition was observed during the temperature sweep. This result indicates that DG-XG association does not change with temperature (i.e., no thermally induced association), while at a higher DG-XG concentration a small transition is visible. The difference between these two mixtures is primarily the DG-XG:CNC ratio. This change might indicate a lack of availability for DG-XG chains to self-associate in response to temperature, possibly due to the low amount of free (or mobile) DG-XG chains as a result of DG-XG-CNC interactions. It should also be noted that the G' value of the 5 g/L DG-XG with 30 g/L CNC gel is higher than that of 5 g/L XGu with 30 g/L CNCs, suggesting that the removal of galactose units induces more interactions between XG chains.

Polarized Optical Microscopy (POM) of XG/CNC Mixtures. Representative transmission POM images of XGu/CNC and DG-XG/CNC mixtures at two ratios (20:1 and 20:10) are displayed in Figure 5. These two ratios correspond to the phase diagram zones where thermal transitions were observed for mixtures containing DG-XG. The mixtures were observed in sealed microscope slides between cross polarizers (with a 530 nm retardation plate) on a heating plate at temperatures from 20 to 60 °C (i.e., below and above the LCST). An isotropic phase appears as a pink homogeneous zone while anisotropic regions are visualized as yellow or blue. Anisotropic phases are likely caused by the formation of zones with higher CNC concentration and denser organization displaying anisotropic arrangement, while isotropic zones correspond to homogeneous dispersions of CNCs at the micrometer to millimeter scale. Dark red zones correspond to denser materials scattering light but with lower or no anisotropy.

The first observation from these images is that no change is seen during the temperature sweep in the samples containing XGu (comparison between Figures 5a,e and 5b,f), which was expected based on the phase diagram and rheological behavior observed. Both at low and high CNC concentrations, the images are superimposable. In the case of DG-XG, no evolution can be seen at low CNC concentration (compare Figures 5c,g), but some differences in the images appeared for high CNC concentrations at the two different temperatures (compare Figures 5d,h). Images of 20 g/L DG-XG with 10 g/L of CNCs display some color changes, as noted with more dark blue areas that indicate more aligned regions, with an increase in temperature. However, from these observations, it can be inferred that the thermal transition does not strongly affect the gel morphology, at least at the submillimeter scale.

In contrast, for both XGu and DG-XG, the CNC concentration appears to be a critical factor controlling gel morphology. Indeed, comparison of the images indicates a significant evolution of the morphology since anisotropic phases are clearly visible at higher concentrations (Figures 5b,f,d,h). Moreover, the structures formed by the XGu/CNC and DG-XG/CNC mixtures are different. The DG-XG/CNC structure appears more reticulated and scattered (Figures 5d,h) while that of XGu/CNC appears to have more extended zones (Figures 5b,f). At lower concentrations, the XGu/CNC sample appears homogeneous, suggesting that CNCs are uniformly dispersed in the polymer mixture (Figures 5a,e). However, in

https://dx.doi.org/10.1021/acs.biomac.0c01521
Biomacromolecules 2021, 22, 743−753

the case of DG-XG/CNC, elongated inhomogeneous structures are visible even at low CNC concentrations (Figures 5c,g), suggesting that DG-XG-CNC interactions and DG-XG self-association lead to macromolecular aggregates with anisotropic structures.

The formation of bright birefringent areas (yellow/blue zones of Figures 5b,d,f,h) in the presence of CNCs indicates an anisotropic distribution of CNCs in the dispersion, creating zones containing CNCs aligned along preferred orientations. The formation of enriched zones when polymers were added to a CNC dispersion has been reported.[23−25,51,52] According to previous work, these zones can be the result of a depletion flocculation process either when the added polymer does not interact with the CNCs[24,25,52] or when polymer adsorption occurs, the increased effective hydrodynamic volume of the CNCs encourages the onset of liquid crystalline self-assembly into optically active phases (i.e., liquid-crystalline liquid) at lower CNC concentrations than normally seen.[23] In the present work, given that both XGu and DG-XG adsorbed to CNCs, as demonstrated by QCM-D, the second mechanism seems more likely. Differences observed from the POM images can be related to the formation of XG-CNC complexes that are crowded and form denser zones due to their larger size. Therefore, the differences between the POM images of XGu and DG-XG indicate that degalactosylation affects the self-assembly process of XG and CNCs.

Conclusions drawn from the POM images are in good agreement with the QCM-D and rheological measurements. Results from QCM-D indicate that more DG-XG adsorbs to CNCs at higher concentrations, tending to form denser structures. This is the result of stronger interactions between the degalactosylated regions of the DG-XG chains, in agreement with our previous results.[53] For XGu, the self-association of XGu chains is lower or unfavorable due to the presence of more galactose substituents. The interaction between DG-XG chains is also supported by rheological measurements where DG-XG displays a higher G' than XGu at all concentrations. Using colloidal probe atomic force microscopy measurements, Stiernstedt et al. concluded that XG displayed strong interaction with cellulose, while also reducing friction due to steric crowding of the surface.[54] Similar conclusions can be drawn from the construction of XG/CNC multilayered thin films.[55,56] The modification of the galactosyl side chain pattern changes XG-CNC interactions, resulting in different morphologies compared to unmodified XG-CNC complexes, promoting larger and denser structures that play a greater role in gel formation and reinforcement.

The overall behavior of DG-XG/CNC hydrogels emphasizes the potential of such polymer/particle systems in future applications since they present a LCST close to the body temperature, similar to other thermoresponsive systems described in the literature, such as poly(*N*-isopropylacrylamide), and poly(ethylene oxide) copolymers.[57,58] Nevertheless, besides displaying an LCST at physiological temperature, injectable thermosensitive systems should also meet several criteria such as good mechanical properties, rapid gelation time, and biocompatibility. Rheological properties of DG-XG/CNC systems have been found to be easily tunable to achieve mechanical properties similar to or higher than those of high concentration DG-XG solutions or alternative synthetic hydrogels.[59−61] Although we have not investigated in detail the DG-XG/CNC system gelation time, it is clearly in the minute range and thus compatible with biomedical application requirements.[59] While both DG-XG and CNCs present low toxicity and biocompatibility, long-term studies would still be valuable.[62,63] Thus, it is likely that implementation of DG-XG/CNC mixtures with a preparation process devoid of chemical reaction or modification will lead to safe and sustainable applicative solutions.

CONCLUSIONS

In this work, we have focused on comparing the interactions of CNCs with partially degalastosylated XG and with XGu displaying a regular galactose ubstitution pattern. Degalactosylation was found to affect the adsorption of DG-XG to CNCs forming a denser layer, as observed by QCM-D. We found that by mixing DG-XG and CNCs, it was possible to achieve thermoresponsive hydrogels with tunable mechanical properties. The thermal transition of the gel occurs at 35 °C and is thus close to human body temperature. In addition to the low toxicity of XG and CNCs and the absence of any hazardous chemistry, these results may pave the way toward new bioinspired hydrogels for medical applications.

ASSOCIATED CONTENT

Supporting Information

The Supporting Information is available free of charge at https://pubs.acs.org/doi/10.1021/acs.biomac.0c01521.

Values of G' and G'' at 20 and 60 °C for heating and cooling cycles; High Pressure Steric Exclusion Chromatography traces and molar mass distribution of XGt, XGu and DG-XG; Evolution of the storage and loss moduli as a function of temperature for XGu and DG-XG; photographs of phases observed in inverted test tubes and QCM-D adsorption data for DG-XG onto CNC-coated sensors measured over 16 h (PDF)

AUTHOR INFORMATION

Corresponding Author

Bernard Cathala − *UR1268 BIA, INRAE, 44300 Nantes, France*; orcid.org/0000-0002-3844-872X; Email: Bernard.cathala@inrae.fr

Authors

Malika Talantikite − *UR1268 BIA, INRAE, 44300 Nantes, France*

Taylor C. Stimpson − *Department of Chemical Engineering, McMaster University, Hamilton, ON L8S 4L7, Canada*

Antoine Gourlay − *UR1268 BIA, INRAE, 44300 Nantes, France*

Sophie Le-Gall − *UR1268 BIA, INRAE, 44300 Nantes, France*

Céline Moreau − *UR1268 BIA, INRAE, 44300 Nantes, France*

Emily D. Cranston − *Department of Chemical Engineering, McMaster University, Hamilton, ON L8S 4L7, Canada; Department of Wood Science and Department of Chemical and Biological Engineering, The University of British Columbia, Vancouver, BC V6T 1Z4, Canada*; orcid.org/0000-0003-4210-9787

Jose M. Moran-Mirabal − *Department of Chemistry and Chemical Biology, McMaster University, Hamilton, ON L8S 4M1, Canada*; orcid.org/0000-0002-4811-3085

Complete contact information is available at: https://pubs.acs.org/10.1021/acs.biomac.0c01521

https://dx.doi.org/10.1021/acs.biomac.0c01521
Biomacromolecules 2021, 22, 743−753

Funding

This work is a contribution to the Labex Serenade program (no. ANR-11-LABX-0064) funded by the "Investissements d'Avenir" program of the French National Research Agency (ANR) through the A*MIDEX project (no. ANR-11-IDEX-0001-02) and of the HOBIT program financed by the Pays de la Loire region. T.C.S. is the recipient of a Queen Elizabeth II Ontario Graduate Scholarship and was partially supported through a Mitacs Globalink Graduate Fellowship. J.M.M. and E.D.C. are recipients of Early Researcher awards from the Ontario Ministry of Research and Innovation. J.M.M. is the Tier 2 Canada Research Chair in Micro and Nanostructured Materials.

Notes

The authors declare no competing financial interest.

■ ACKNOWLEDGMENTS

Nadège Beury and Bérengère Marais are warmly acknowledged for their excellent technical support.

■ REFERENCES

(1) Park, Y. B.; Cosgrove, D. J. A Revised Architecture of Primary Cell Walls Based on Biomechanical Changes Induced by Substrate-Specific Endoglucanases. *Plant Physiol.* **2012**, *158* (4), 1933−1943.
(2) Park, Y. B.; Cosgrove, D. J. Xyloglucan and its Interactions with Other Components of the Growing Cell Wall. *Plant Cell Physiol.* **2015**, *56* (2), 180−194.
(3) Hayashi, K.; Maclachlan, G. Pea Xyloglucan and Cellulose. *Plant Physiol.* **1984**, *75*, 596−604.
(4) Hayashi, T.; Marsden, M. P. F.; Delmer, D. P. Pea xyloglucan and cellulose: xyloglucan-cellulose interactions in vitro and in vivo. *Plant Physiol.* **1987**, *83*, 384−389.
(5) Benselfelt, T.; Cranston, E. D.; Ondaral, S.; Johansson, E.; Brumer, H.; Rutland, M. W.; Wågberg, L. Adsorption of Xyloglucan onto Cellulose Surfaces of Different Morphologies: An Entropy-Driven Process. *Biomacromolecules* **2016**, *17* (9), 2801−2811.
(6) Villares, A.; Moreau, C.; Dammak, A.; Capron, I.; Cathala, B. Kinetic aspects of the adsorption of xyloglucan onto cellulose nanocrystals. *Soft Matter* **2015**, *11* (32), 6472−6481.
(7) Villares, A.; Bizot, H.; Moreau, C.; Rolland-Sabate, A.; Cathala, B. Effect of xyloglucan molar mass on its assembly onto the cellulose surface and its enzymatic susceptibility. *Carbohydr. Polym.* **2017**, *157*, 1105−1112.
(8) Kishani, S.; Vilaplana, F.; Ruda, M.; Hansson, P.; Wågberg, L. The influence of solubility on the adsorption of different Xyloglucan fractions at Cellulose Water Interfaces. *Biomacromolecules* **2020**, *21*, 772.
(9) Klemm, D.; Kramer, F.; Moritz, S.; Lindström, T.; Ankerfors, M.; Gray, D.; Dorris, A. Nanocelluloses: A New Family of Nature-Based Materials. *Angew. Chem., Int. Ed.* **2011**, *50* (24), 5438−5466.
(10) Merindol, R.; Diabang, S.; Felix, O.; Roland, T.; Gauthier, C.; Decher, G. Bio-Inspired Multiproperty Materials: Strong, Self-Healing, and Transparent Artificial Wood Nanostructures. *ACS Nano* **2015**, *9* (2), 1127−1136.
(11) Paulraj, T.; Riazanova, A. V.; Yao, K.; Andersson, R. L.; Mullertz, A.; Svagan, A. J. Bioinspired Layer-by-Layer Microcapsules Based on Cellulose Nanofibers with Switchable Permeability. *Biomacromolecules* **2017**, *18* (4), 1401−1410.
(12) Chin, K. M.; Ting, S. S.; Ong, H. L.; Omar, M. Surface functionalized nanocellulose as a veritable inclusionary material in contemporary bioinspired applications: A review. *J. Appl. Polym. Sci.* **2018**, *135* (13), 19.
(13) Mittal, N.; Benselfelt, T.; Ansari, F.; Gordeyeva, K.; Roth, S. V.; Wagberg, L.; Soderberg, L. D. Ion-Specific Assembly of Strong, Tough, and Stiff Biofibers. *Angew. Chem., Int. Ed.* **2019**, *58* (51), 18562−18569.
(14) Habibi, Y.; Lucia, L. A.; Rojas, O. J. Cellulose Nanocrystals: Chemistry, Self-Assembly, and Applications. *Chem. Rev.* **2010**, *110* (6), 3479−3500.
(15) Moreau, C.; Villares, A.; Capron, I.; Cathala, B. Tuning supramolecular interactions of cellulose nanocrystals to design innovative functional materials. *Ind. Crops Prod.* **2016**, *93*, 96−107.
(16) Grishkewich, N.; Mohammed, N.; Tang, J. T.; Tam, K. C. Recent advances in the application of cellulose nanocrystals. *Curr. Opin. Colloid Interface Sci.* **2017**, *29*, 32−45.
(17) De France, K. J.; Hoare, T.; Cranston, E. D. Review of Hydrogels and Aerogels Containing Nanocellulose. *Chem. Mater.* **2017**, *29* (11), 4609−4631.
(18) Matanović, M. R.; Kristl, J.; Grabnar, P. A. Thermoresponsive polymers: Insights into decisive hydrogel characteristics, mechanisms of gelation, and promising biomedical applications. *Int. J. Pharm.* **2014**, *472* (1), 262−275.
(19) Rose, S.; Prevoteau, A.; Elzière, P.; Hourdet, D.; Marcellan, A.; Leibler, L. Nanoparticle solutions as adhesives for gels and biological tissues. *Nature* **2014**, *505* (7483), 382−385.
(20) Appel, E. A.; Tibbitt, M. W.; Webber, M. J.; Mattix, B. A.; Veiseh, O.; Langer, R. Self-assembled hydrogels utilizing polymer-nanoparticle interactions. *Nat. Commun.* **2015**, *6*, 9.
(21) Appel, E. A.; Scherman, O. A. A nanoparticle solution. *Nat. Mater.* **2014**, *13* (3), 231−232.
(22) Wang, Q.; Mynar, J. L.; Yoshida, M.; Lee, E.; Lee, M.; Okuro, K.; Kinbara, K.; Aida, T. High-water-content mouldable hydrogels by mixing clay and a dendritic molecular binder. *Nature* **2010**, *463* (7279), 339−343.
(23) Hu, Z.; Cranston, E. D.; Ng, R.; Pelton, R. Tuning Cellulose Nanocrystal Gelation with Polysaccharides and Surfactants. *Langmuir* **2014**, *30* (10), 2684−2692.
(24) Oguzlu, H.; Boluk, Y. Interactions between cellulose nanocrystals and anionic and neutral polymers in aqueous solutions. *Cellulose* **2017**, *24* (1), 131−146.
(25) Oguzlu, H.; Danumah, C.; Boluk, Y. Colloidal behavior of aqueous cellulose nanocrystal suspensions. *Curr. Opin. Colloid Interface Sci.* **2017**, *29*, 46−56.
(26) Prabaharan, M.; Mano, J. F. Stimuli-responsive hydrogels based on polysaccharides incorporated with thermo-responsive polymers as novel biomaterials. *Macromol. Biosci.* **2006**, *6* (12), 991−1008.
(27) Pacheco, D. P.; Marcello, E.; Bloise, N.; Sacchetti, A.; Brenna, E.; Visai, L.; Petrini, P. Design of Multifunctional Polysaccharides for Biomedical Applications: A Critical Review. *Curr. Org. Chem.* **2018**, *22* (12), 1222−1236.
(28) Graham, S.; Marina, P. F.; Blencowe, A. Thermoresponsive polysaccharides and their thermoreversible physical hydrogel networks. *Carbohydr. Polym.* **2019**, *207*, 143−159.
(29) Darge, H. F.; Andrgie, A. T.; Tsai, H.-C.; Lai, J.-Y. Polysaccharide and polypeptide based injectable thermo-sensitive hydrogels for local biomedical applications. *Int. J. Biol. Macromol.* **2019**, *133*, 545−563.
(30) Shirakawa, M.; Yamatoya, K.; Nishinari, K. Tailoring of xyloglucan properties using an enzyme. *Food Hydrocolloids* **1998**, *12* (1), 25−28.
(31) Azzam, F.; Siqueira, E.; Fort, S.; Hassaini, R.; Pignon, F.; Travelet, C.; Putaux, J.-L.; Jean, B. Tunable Aggregation and Gelation of Thermoresponsive Suspensions of Polymer-Grafted Cellulose Nanocrystals. *Biomacromolecules* **2016**, *17* (6), 2112−2119.
(32) Risteen, B.; Delepierre, G.; Srinivasarao, M.; Weder, C.; Russo, P.; Reichmanis, E.; Zoppe, J. Thermally Switchable Liquid Crystals Based on Cellulose Nanocrystals with Patchy Polymer Grafts. *Small* **2018**, *14* (46), 1870218.
(33) Kedzior, S. A.; Zoppe, J. O.; Berry, R. M.; Cranston, E. D. Recent advances and an industrial perspective of cellulose nanocrystal functionalization through polymer grafting. *Curr. Opin. Solid State Mater. Sci.* **2019**, *23* (2), 74−91.
(34) McKee, J. R.; Hietala, S.; Seitsonen, J.; Laine, J.; Kontturi, E.; Ikkala, O. Thermoresponsive Nanocellulose Hydrogels with Tunable Mechanical Properties. *ACS Macro Lett.* **2014**, *3* (3), 266−270.

https://dx.doi.org/10.1021/acs.biomac.0c01521
Biomacromolecules 2021, 22, 743−753

(35) Gicquel, E.; Martin, C.; Gauthier, Q.; Engstrom, J.; Abbattista, C.; Carlmark, A.; Cranston, E. D.; Jean, B.; Bras, J. Tailoring Rheological Properties of Thermoresponsive Hydrogels through Block Copolymer Adsorption to Cellulose Nanocrystals. *Biomacromolecules* **2019**, *20* (7), 2545−2556.
(36) Reid, M. S.; Villalobos, M.; Cranston, E. D. Benchmarking Cellulose Nanocrystals: From the Laboratory to Industrial Production. *Langmuir* **2017**, *33* (7), 1583−1598.
(37) Brun-Graeppi, A.; Richard, C.; Bessodes, M.; Scherman, D.; Narita, T.; Ducouret, G.; Merten, O. W. Study on the sol-gel transition of xyloglucan hydrogels. *Carbohydr. Polym.* **2010**, *80* (2), 555−562.
(38) Blakeney, A. B.; Harris, P. J.; Henry, R. J.; Stone, B. A. 113, 291−299, A simple and rapid preparation of alditol acetates for monosaccharide analysis. *Carbohydr. Res.* **1983**, *113*, 291−299.
(39) Dervilly-Pinel, G.; Tran, V.; Saulnier, L. Investigation of the distribution of arabinose residues on the xylan backbone of water-soluble arabinoxylans from wheat flour. *Carbohydr. Polym.* **2004**, *55* (2), 171−177.
(40) Sakakibara, C. N.; Sierakowski, M. R.; Chassenieux, C.; Nicolai, T.; de Freitas, R. A. Xyloglucan gelation induced by enzymatic degalactosylation; kinetics and the effect of the molar mass. *Carbohydr. Polym.* **2017**, *174*, 517−523.
(41) de Freitas, R. A.; Busato, A. P.; Mitchell, D. A.; Silveira, J. L. M. Degalatosylation of xyloglucan: Effect on aggregation and conformation, as determined by time dependent static light scattering, HPSEC-MALLS and viscosimetry. *Carbohydr. Polym.* **2011**, *83* (4), 1636−1642.
(42) Talantikite, M.; Beury, N.; Moreau, C.; Cathala, B. Arabinoxylan/Cellulose Nanocrystal Hydrogels with Tunable Mechanical Properties. *Langmuir* **2019**, *35* (41), 13427−13434.
(43) Urena-Benavides, E. E.; Ao, G. Y.; Davis, V. A.; Kitchens, C. L. Rheology and Phase Behavior of Lyotropic Cellulose Nanocrystal Suspensions. *Macromolecules* **2011**, *44* (22), 8990−8998.
(44) Tanaka, H.; Meunier, J.; Bonn, D. Nonergodic states of charged colloidal suspensions: Repulsive and attractive glasses and gels. *Phys. Rev. E* **2004**, *69* (3), 6.
(45) Nordenström, M.; Fall, A.; Nyström, G.; Wågberg, L. Formation of Colloidal Nanocellulose Glasses and Gels. *Langmuir* **2017**, *33* (38), 9772−9780.
(46) de Freitas, R. A.; Spier, V. C.; Sierakowski, M. R.; Nicolai, T.; Benyahia, L.; Chassenieux, C. Transient and quasi-permanent networks in xyloglucan solutions. *Carbohydr. Polym.* **2015**, *129*, 216−223.
(47) Dammak, A.; Quemener, B.; Bonnin, E.; Alvarado, C.; Bouchet, B.; Villares, A.; Moreau, C.; Cathala, B. Exploring Architecture of Xyloglucan Cellulose Nanocrystal Complexes through Enzyme Susceptibility at Different Adsorption Regimes. *Biomacromolecules* **2015**, *16* (2), 589−596.
(48) Spalla, O. Nanoparticle interactions with polymers and polyelectrolytes. *Curr. Opin. Colloid Interface Sci.* **2002**, *7* (3), 179−185.
(49) Spalla, O.; Cabane, B. Growth of colloidal aggregates through polymer bridging. *Colloid Polym. Sci.* **1993**, *271* (4), 357−371.
(50) Alexander, S. Polymer adsorption on small spheres-scaling approach. *J. Phys.* **1977**, *38* (8), 977−981.
(51) Beck-Candanedo, S.; Viet, D.; Gray, D. G. Induced Phase Separation in Low-Ionic-Strength Cellulose Nanocrystal Suspensions Containing High-Molecular-Weight Blue Dextrans. *Langmuir* **2006**, *22* (21), 8690−8695.
(52) Boluk, Y.; Zhao, L.; Incani, V. Dispersions of Nanocrystalline Cellulose in Aqueous Polymer Solutions: Structure Formation of Colloidal Rods. *Langmuir* **2012**, *28* (14), 6114−6123.
(53) Stimpson, T. C.; Cathala, B.; Moreau, C.; Moran-Mirabal, J. M.; Cranston, E. D. Xyloglucan Structure Impacts the Mechanical Properties of Xyloglucan-Cellulose Nanocrystal Layered Films - a Buckling-Based Study. *Biomacromolecules* **2020**, *21* (9), 3898−3908.
(54) Stiernstedt, J.; Brumer, H.; Zhou, Q.; Teeri, T. T.; Rutland, M. W. Friction between cellulose surfaces and effect of xyloglucan adsorption. *Biomacromolecules* **2006**, *7* (7), 2147−2153.
(55) Winter, H. T.; Cerclier, C.; Delorme, N.; Bizot, H.; Quemener, B.; Cathala, B. Improved Colloidal Stability of Bacterial Cellulose Nanocrystal Suspensions for the Elaboration of Spin-Coated Cellulose-Based Model Surfaces. *Biomacromolecules* **2010**, *11* (11), 3144−3151.
(56) Cerclier, C.; Cousin, F.; Bizot, F.; Moreau, C.; Cathala, C. Elaboration of Spin-Coated Cellulose-Xyloglucan Multilayered Thin Films. *Langmuir* **2010**, *26* (22), 17248−1725.
(57) Schild, H. G. Poly (N-isopropylacrylamide)- experiment, theory and application. *Prog. Polym. Sci.* **1992**, *17* (2), 163−249.
(58) Radivojsa, M.; Grabnar, I.; Grabnar, P. A. Thermoreversible in situ gelling poloxamer-based systems with chitosan nanocomplexes for prolonged subcutaneous delivery of heparin: Design and in vitro evaluation. *Eur. J. Pharm. Sci.* **2013**, *50* (1), 93−101.
(59) Zhang, E.; Li, J.; Zhou, Y.; Che, P.; Ren, B.; Qin, Z.; Ma, L.; Cui, J.; Sun, H.; Yao, F. Biodegradable and injectable thermoreversible xyloglucan based hydrogel for prevention of postoperative adhesion. *Acta Biomater.* **2017**, *55*, 420−433.
(60) Zhang, Z.; Ni, J.; Chen, L.; Yu, L.; Xu, J.; Ding, J. Biodegradable and thermoreversible PCLA-PEG-PCLA hydrogel as a barrier for prevention of post-operative adhesion. *Biomaterials* **2011**, *32* (21), 4725−4736.
(61) Yu, L.; Hu, H.; Chen, L.; Bao, X.; Li, Y.; Chen, L.; Xu, G.; Ye, X.; Ding, J. Comparative studies of thermogels in preventing post-operative adhesions and corresponding mechanisms. *Biomater. Sci.* **2014**, *2* (8), 1100−1109.
(62) De France, K. J.; Yager, K. G.; Chan, K. J. W.; Corbett, B.; Cranston, E. D.; Hoare, T. Injectable Anisotropic Nanocomposite Hydrogels Direct in Situ Growth and Alignment of Myotubes. *Nano Lett.* **2017**, *17* (10), 6487−6495.
(63) Roman, M. Toxicity of Cellulose Nanocrystals: A Review. *Ind. Biotechnol.* **2015**, *11* (1), 25−30.

https://dx.doi.org/10.1021/acs.biomac.0c01521
Biomacromolecules 2021, 22, 743−753